HHS Public Access

Author manuscript

Mol Cancer Ther. Author manuscript; available in PMC 2022 April 01.

Published in final edited form as:

Mol Cancer Ther. 2021 October ; 20(10): 2035–2048. doi:10.1158/1535-7163.MCT-20-0973.

KIT^{low} Cells Mediate Imatinib Resistance in Gastrointestinal Stromal Tumor

Sudeep Banerjee[1,2,3,*], **Hyunho Yoon**[1,3,*], **Stephanie Ting**[3,4], **Chih-Min Tang**[1,3], **Mayra Yebra**[1,3], **Alexander T. Wenzel**[3,4], **Huwate Yeerna**[3,4], **Jill P. Mesirov**[3,4], **Robert J. Wechsler-Reya**[5], **Pablo Tamayo**[3,4,6], **Jason K. Sicklick**[1,3]

[1]Department of Surgery, Division of Surgical Oncology, University of California, San Diego

[2]Department of Surgery, University of California, Los Angeles

[3]Moores Cancer Center, University of California, San Diego

[4]Department of Medicine, Division of Medical Genetics, University of California, San Diego

[5]Sanford Burnham Prebys Medical Discovery Institute, La Jolla

[6]UCSD Center for Novel Therapeutics

Abstract

Gastrointestinal stromal tumor (GIST) is commonly driven by oncogenic *KIT* mutations that are effectively targeted by imatinib, a tyrosine kinase inhibitor (TKI). However, IM does not cure GIST and adjuvant therapy only delays recurrence in high-risk tumors. We hypothesized that GIST contains cells with primary imatinib resistance that may represent a reservoir for disease persistence. Here, we report a subpopulation of CD34^{+}KIT^{low} human GIST cells that have intrinsic imatinib resistance. These cells possess cancer stem cell-like expression profiles and behavior, including self-renewal and differentiation into CD34^{+}KIT^{high} progeny that are sensitive to imatinib treatment. We also found that TKI treatment of GIST cell lines led to induction of stem-cell associated transcription factors (*OCT4* and *NANOG*) and concomitant enrichment of the CD34^{+}KIT^{low} cell population. Using a data-driven approach, we constructed a transcriptomic-oncogenic map (Onco-GPS) based on the gene expression of 134 GIST samples to define pathway activation during GIST tumorigenesis. Tumors with low KIT expression had overexpression of cancer stem cell gene signatures consistent with our *in vitro* findings. Additionally, these tumors had activation of the Gas6/AXL pathway and NF-κB signaling gene signatures. We evaluated these targets *in vitro* and found that primary imatinib-resistant GIST cells were effectively targeted with either single agent bemcentinib (AXL inhibitor) or bardoxolone (NF-κB inhibitor), as well as with either agent in combination with imatinib. Collectively, these findings suggest that CD34^{+}KIT^{low} cells represent a distinct, but targetable, subpopulation in human GIST that may represent a novel mechanism of primary TKI resistance, as well as a target for overcoming disease persistence following TKI therapy.

Corresponding author: Jason K. Sicklick, MD, FACS, Professor of Surgery, Department of Surgery, Division of Surgical Oncology, University of California, San Diego, UC San Diego Health Sciences, 3855 Health Sciences Drive, Room 4311, Mail Code 0987, La Jolla, CA 92093-0987, Tel: 858-822-3967, Fax: 858-228-5153, jsicklick@health.ucsd.edu.

*Contributed equally.

Keywords

GIST; KIT; c-KIT; cancer stem cells; disease persistence; TKI resistance

Background

Gastrointestinal stromal tumor (GIST) is the most common mesenchymal tumor of the gastrointestinal tract.(1) The treatment of GIST provided proof of principle for precision medicine in solid tumors as oncogenic driver mutations in the *KIT* gene were identified and targeted with the tyrosine kinase inhibitor (TKI), imatinib (IM). Despite this landmark discovery, clinical trials show that 40% of primary localized GISTs develop recurrence within 5 years.(2) In clinical trials, high-risk patients begin developing recurrences between 8 to 12 months after stopping adjuvant imatinib, leading to near convergence of all survival curves irrespective of the length of imatinib therapy.(3–5) The later lines of FDA-approved anti-GIST TKIs (i.e., sunitinib, regorafenib, and ripretinib) can provide additional survival benefit, but disease control is often short-lived.(6,7) These observations suggest that the paradigm of targeting *KIT* oncogene addiction is fundamentally limited.

TKI resistance is mediated by acquired and *de novo* causes. Acquired resistance is the most common mechanism and involves acquisition of secondary *KIT* mutations following imatinib treatment. These mutations are well characterized and tend to cluster in either the ATP-binding pocket or the activation loop of KIT, impairing the ability of imatinib to bind KIT.(8) Contrastingly, *de novo,* or primary resistance, is seen in 10-20% of GISTs. In general, this TKI sensitivity is entirely determined by specific alterations within driver mutations.(9–11) While 60-70% of all sporadic GISTs have activating genomic alterations in *KIT,* certain alterations (i.e., *KIT* exon 17) confer primary resistance to imatinib. Similarly, 10-15% of GISTs have activating genomic alterations in *PDGFRA* that are frequently TKI sensitive, with the exception of *PDGFRA* D842V mutants that are intrinsically imatinib resistant, but respond to the newly FDA-approved agent, avapritinib.(10,12,13) The remainder of GISTs are driven by a heterogenous group of alterations, but are frequently TKI resistant. These include 15% with activation of the *RAS* pathway (*K/H/N-RAS*, *BRAF*, *NF1*) and 7% arising from mutations or epimutations in *SDHx* subunits (A, B, C, or D), and kinase fusions (*ETV6-NTRK3*, *FGFR1-TACC1*, or *FGFR1-HOOK3*).(10,13–18) Despite variable genomics, the putative cell of origin – the interstitial cell of Cajal (ICC) (19–21) – appears to be the same for all subgroups of the disease.(10,22)

On the basis that cancer stem cells (CSCs) arise from and resemble their cell of origin,(21,23) genetic subtypes of a cancer may possess similar CSCs that may be responsive to killing by similar therapies. Currently, very little is known about GIST CSCs, and therefore effective agents for targeting them remain undetermined. Studies in a mouse model of GIST suggest that $KIT^{low}CD34^{+}$ cells may represent IM-resistant murine GIST CSCs.(24) While all anti-KIT TKIs hit the “right” target in mature *KIT*-mutant GIST cells, they do not target KIT^{low} cells, a possible cellular reservoir for disease persistence and recurrence.

In the present study, we sought to identify $KIT^{low}CD34^{+}$ GIST cells and to define the molecular properties of these GIST cells isolated from human GISTs bearing heterogenous

KIT mutations. We then performed a bioinformatic-driven approach to determine distinct oncogenic states that predominate within the KIT^{low} GIST subpopulation. Lastly, we tested putative candidate therapies for cytotoxicity of KIT^{low} GIST cells. On this basis, we hypothesized that human $KIT^{low}CD34^{+}$ cells are an intrinsically TKI-resistant subpopulation that exists within primary human GIST, and can mediate tumor recurrence and disease progression.

Methods

Reagents

Cell culture media and reagents were purchased from Mediatech (Manassas, VA). Primary and secondary antibodies for immunoblotting, immunofluorescent staining, and immunohistochemistry (IHC) are described in the Supplementary Table 1. OPAL 4-color manual IHC Kit was purchased from Akoya Biosciences (Marlborough, MA). iScript cDNA synthesis kit and iTaq universal SYBR Green supermix were purchased from Bio-Rad Laboratories (Hercules, CA). Dimethyl sulfoxide (DMSO), poly(2-hydroxyethyl methacrylate) (poly-HEMA), and MTT reagent, 3-(4, 5-dimethylthiazol-2-yl)-2,5-diphenyltetrazolium bromide, were purchased from Sigma-Aldrich (St. Louis, MO). Transwell plates were purchased from Corning (Lowell, MA). CellTiter-Glo (CTG) luminescent cell viability assay was purchased from Promega (Madison, WI). BCA protein assay, the Western Blot stripping buffer, and an enhanced chemiluminescence system for western blot detection were purchased from Thermo Scientific (Waltham, MA). Bemcentinib/BEM, bardoxlone/BARD, and Nocodazole were purchased from Selleckchem (Houston, TX). Imatinib (IM) was provided by Novartis Pharmaceuticals (East Hanover, NJ). Propidium iodide (PI) is from Roche Applied Science (Indianapolis, IN). ALDEFLUOR kit was purchased from STEMCELL Technologies (Cambridge, MA). The RNeasy Kit was purchased from Qiagen (Germantown, MD). The human tumor dissociation kit is from Miltenyi Biotec (Auburn, CA).

Human GIST Source

Tumor acquisition and banking under our IRB-approved protocol (#181755) is routinely performed for all surgical procedures at UC San Diego Moores Cancer Center. Informed consent was obtained from all patients for tissue collection. Resected tumors were first submitted to Moores Pathology for diagnostic workup. The Biorepository and Tissue Technology Shared Resource (BTTSR) at Moores Cancer Center then acquired and distributed excess tumor tissue for research purposes. Table 1 lists demographic information of 4 GIST patients in this study who underwent operations. Clinical diagnosis of GIST employed tissue staining including hematoxylin and eosin (H&E), KIT and ANO1. The immunohistological diagnoses were confirmed under light microscopy by an experienced pathologist. Tumor samples from these 4 patients were used for flow cytometry assays and immunofluorescent staining as described below.

Tumor Dissociation

Resected fresh tumors were cut into fine pieces and processed into single-cell suspensions using the human tumor dissociation kit (Miltenyi Biotec, Auburn, CA). Briefly, tumor tissue

was digested with a proprietary enzyme mixture and mechanically dissociated using the gentleMACS Dissociator (Miltenyi Biotec) following the manufacturer's instructions for the tough tumor settings. Undigested tissue was removed by passing through a 70-micron filter. Dissociated tumor cells were collected and counted with a TC20 Automated Cell Counter (Bio-Rad). Cell viability was checked using 0.4% trypan blue dye.

GIST Cell and Tumorsphere Cultures

The GIST-T1 line containing *KIT* exon 11 (V560-Y579Δ5) mutation(25) was cultured in Dulbecco's modified Eagle's medium (DMEM; Gibco) with 10% FBS. The GIST882 line containing *KIT* exon 13 (K642E) mutation(26) was cultured in Roswell Park Memorial Institute (RPMI 1640; Gibco) with 20% FBS. All cell culture media were supplemented with 1% penicillin/streptomycin (Mediatech) and 2 mM glutamine (Mediatech). All cell lines were maintained in a humidified incubator with 5% CO_2 at 37°C. All cell lines were confirmed to be negative for mycoplasma contamination. For tumorsphere culture, GIST-T1 cells were seeded at a density of 2.5 x 10^5 cells/well in poly-HEMA-coated 6-well plates, and allowed to grow as spheres for indicated time.

Two-step Real-time Quantitative RT-PCR

Human GIST snap-frozen tumor was processed with a tissue homogenizer in RLT lysis buffer (Qiagen, Germantown, MD). Total RNA from tissue homogenates or cell pellets was prepared using the RNeasy Kit (Qiagen) according to manufacturer's instructions. Reverse transcription with iScript cDNA synthesis kit (Bio-Rad) and quantitative real-time PCR conducted with iTaq universal SYBR Green supermix (Bio-Rad). Samples were run on a CFX96 real-time system (Bio-Rad) with the following PCR parameters: denaturing at 95°C for 30 seconds followed by 40 cycles of 10-second denaturation at 95°C, 30-second annealing at the optimal primer annealing temperatures, and 10-second extension at 72°C. Primers specific for genes of interest and the beta-actin and cyclophilin A housekeeping genes are in Supplementary Table 1. The threshold cycle (Ct) values from triplicated samples were automatically generated after each run. Target gene levels based on Ct values are presented as a ratio to levels detected in the control samples, according to the ΔΔCt method.(27)

Immunoblotting

Monolayer cells were lysed and scraped in RIPA buffer (Cell Signaling Technology, Danvers, MA) containing Halt Protease and Phosphatase Inhibitor Cocktail (ThermoFisher Scientific); while tumorsphere pellets were directly lysed in the same buffer/inhibitor solution. Whole cell lysates were cleared by centrifugation at 14,000 rpm for 30 min and protein was quantified using the BCA protein assay (ThermoFisher Scientific). Protein lysates were resolved on a 4–12% Bis-Tris gel (Life Technologies, Carlsbad, CA) and transferred to a polyvinylidene difluoride (PVDF) membrane which was blocked for 1 hour at room temperature. The membrane was incubated with indicated primary antibody (1:1,000) overnight at 4°C; then followed with 1 h incubation of horseradish peroxidase (HRP)-conjugated secondary antibody (1:5,000) at room temperature. Protein bands were detected using the Pierce enhanced chemiluminescence (ECL) Western blotting detection system (ThermoFisher Scientific). Bound antibodies were removed from membranes using

Restore PLUS Western Blot Stripping Buffer (ThermoFisher Scientific). Then the membrane was re-probed with the alpha-tubulin antibody (Cell Signaling Technology) for loading controls and detected by an HRP-conjugated goat anti-mouse IgG (1:5,000, Jackson ImmunoResearch Laboratories, West Grove, PA) and the Pierce ECL reagents.

Flow Cytometry (FCM)/ Fluorescence-activated cell sorting (FACS)

GIST882 cells were harvested, counted using a TC20 cell counter (Bio-Rad), and stained with CD34-PE and CD117-APC (both from BD Biosciences) for 30 minutes on ice in the dark. To evaluate cell viability, propidium iodide (PI, Roche Applied Science, Indianapolis, IN) was added to samples immediately before analysis. Stained cells were analyzed using a BD FACSDiva cell sorter (BD Biosciences) with 10,000 events collected for each sample. GIST882 cells were treated with imatinib (IM) with the specified final concentration for 48-72 hours as indicated in figure legends. After treatment, cells were harvested, counted, and stained as described above. The 3 subpopulations were identified and defined as following: stem cells as KIT^{low} $CD34^{+}$, immature cells as KIT^{high} $CD34^{+}$, and mature cells as KIT^{high} $CD34^{-}$. Two subpopulations, stem cells and immature cells, were sorted and subjected to downstream experiments named as KIT^{low} and KIT^{high}, respectively.

For single-cell sorting, individual KIT^{low} (N=48) or KIT^{high} (N=48) cells were sorted directly into a 96-well plate and co-cultured in regular growth media with unsorted GIST882 (10,000 cells/well) on a Transwell top for 2 weeks; then the Transwell top was discarded and sorted cells continued to grow for additional 3 weeks. At the end of 5 weeks, cell proliferation was determined by CellTiter-Glo (CTG) assay as described below and expressed as relative fluorescent units (RFU).

Cell Viability Assay

GIST-T1 and GIST882 cells were seeded in 96-well plates and treated in triplicate with indicated compounds for 72 or 120 hours, respectively. MTT reagent, 3-(4, 5-dimethylthiazol-2-yl)-2,5-diphenyltetrazolium bromide (Sigma-Aldrich), was added to cells and then incubated for 4 hours at 37°C. Dimethyl sulfoxide (DMSO, Sigma-Aldrich) was used to dissolve purple formazan product. The absorbance was read at 560 nm to measure cell viability. The background absorbance was determined from wells with media only.

For sequential treatment experiments, GIST882 and GIST-T1 cells were treated for a total of 6 days in sextuplicate for each condition. More specifically, imatinib added to GIST cells for 3 days. After imatinib treatment, remaining cells in wells were subjected to various conditions for an additional 3 days: 0.1% DMSO, IM, BARD, BEM, (IM+BARD), or (IM+BEM). All groups were analyzed by MTT assay to determine cell viability as described above. The following conditions were set as controls of 100% viability: cells treated with DMSO for 3 days (for the 3-day group) or DMSO 6 days (for the 6-day group).

Cell Cycle Analysis

GIST-T1 and GIST882 cells were grown to 70-80% confluency and harvested using Trypsin. Cells were then treated with RNAse (10 μg/ml) for 10 min at room temperature followed by propidium iodide (0.5 mg/ml in PBS) for 30 min at 37°C in the dark. Cell cycle arrest was

achieved by nocodazole treatment (50 ng/mL) for 24 hours in regular growth media prior to the aforementioned steps. Cells were analyzed by BD FACSAria™ Flow Cytometer.

ALDEFLUOR Assay

ALDH isoform activity analysis was performed using the ALDEFLUOR kit (STEMCELL technologies). Briefly, GIST882 cell pellets or dissociated tumor tissue were collected and resuspended in Aldefluor assay buffer. Cells were then incubated with BODIPY-aminoacetaldehyde (BAAA) which is a fluorescent substrate for ALDH. Control tubes were set as BAAA added to cells in the presence of N,N-diethylaminobenzaldehyde (DEAB), an inhibitor of ALDH enzymes. ALDH-positive (i.e. $ALDH^{high}$) versus ALDH-negative (i.e. $ALDH^{low}$) cells were analyzed and separated using a BD FACSDiva cell sorter.

Immunofluorescence and Confocal Microscopy

GIST tumorsphere pellets were embedded in optimal cutting temperature (OCT) compound prior to frozen sectioning. Sections were fixed with 4% paraformaldehyde, permeabilized with 0.3% Triton X-100, blocked with 5% normal donkey serum in PBS, and labelled with anti-OCT4 (ab200834), anti-NANOG (ab109250), or Ki-67 antibody (ab15580). Co-staining of ≥ 2 antibodies was performed with the OPAL 4-color manual IHC Kit (Akoya Biosciences) following the manufacturer's instructions. Slides were incubated with Alexa Fluor-conjugated secondary antibodies (ThermoFisher Scientific) and 4′,6-diamidino-2-phenylindole (DAPI) at room temperature in the dark and mounted in ProLongGold antifademountant (ThermoFisher Scientific). Immunofluorescence images were captured using a Nikon Confocal A1R Microscope (Nikon, Melville, NY). In addition, fresh-frozen OCT-embedded tumor tissues were sectioned, fixed, stained, and imaged as described above.

In vivo Spleen-to-liver metastasis model

Five-week-old male nude mice were purchased from the Jackson Laboratory (Bar Harbor, ME). mCherry-conjugated T1 cells were treated with 10 nM IM for 4 days then sorted for KIT^{low} or KIT^{high} cells. 1 x 10^6 cells resuspended with Hanks' Balanced Salt Solution (HBSS) were injected into the spleen (KIT^{low}: n=3, KIT^{high}: n=3). After 3 weeks, all mice were sacrificed. The harvested livers from each mouse were analyzed using the IVIS imaging system (Xenogen) in an unblinded manner. The IVIS signals were graphed by total photon flux (p/s). All animal experiments were conducted in accordance with protocol S11020 approved by the Institutional Animal Care and Use Committee of University of California, San Diego.

Bioinformatics Analysis

Gene Set Enrichment Analysis (GSEA) was performed on paired data (pre- and post-IM) from 18 patients in RTOG 0132 study using publicly available data (GSE1596636).(28–30) Human GIST RNASeq data from 75 GIST samples generated in previous study are accessible from the Sequencing Read Archive (Accession number PRJNA521803).(31)

Onco-GPS

The methodology to define GIST states follows our original Onco-GPS approach.(32) The method starts by defining a group of GIST-relevant gene sets (see Supplementary Table 2) from our MSigDB (*Molecular Signatures Database*(33,34)). These were chosen based on the current molecular, biological and genomic understanding of the disease. These gene sets define a total of 3,675 GIST-relevant genes that we believe are relevant and representative of transcriptional changes in GIST. The mRNA profiles of these genes are selected in 4 GIST datasets(31,35–37) representing 134 GISTs. Genetically diverse GIST samples were utilized to study KIT^{low} cells in a genotype-agnostic manner. This is a feasible approach because non-*KIT* mutant GIST often highly express wild-type KIT protein.(10) Additionally, non-*KIT* mutant GISTs are known to have overlapping downstream targets as *KIT*-mutant GIST and promote tumorigenesis via parallel pathways.(38) These datasets, sharing the same selected GIST-relevant genes, are then decomposed using a parallel Non-Negative Matrix Factorization (NMF) algorithm(39) that produces a common *genes vs. components* matrix (W) and 4 *components vs. samples* matrices ($H_{1\text{-}4}$). The output lower rank matrices from the NMF decomposition (W, $H_{1\text{-}4}$) represent the most coherent patterns of gene expression across the many GIST in the input datasets. The W matrix provides the weight of each gene in each component, and the matrix H provides the combination of components to make each of the original sample profiles. In this way, the NMF algorithm deconvolves the functional consequences of GIST oncogene activation and produces a set of 5 transcriptional components. The decomposition treats the 4 input datasets independently and in parallel so the model is able to find common transcriptional components shared by the datasets without one dominating the other as they all get some dedicated amount of numerical "real state" in the output ($H_{1\text{-}4}$ matrices). Once the Onco-GPS transcriptional components have been divided they are used to cluster the GIST samples in the 4 datasets in order to define oncogenic states (Supplementary Fig. 5). This is accomplished using a hierarchical clustering algorithm(32). The components and oncogenic states are displayed in a 2D layout (Onco-GPS map) following the Onco-GPS method (Fig 5).

Annotating the Onco-GPS components and single-sample GSEA Analysis.

This computational characterization is based on measuring the degree of association between each transcriptional component and different types of genomic features that have been profiled for the same tumor samples. To estimate the degree of association we will use a rescaled mutual information metric: the Information Coefficient (IC). The IC is a non-linear correlation coefficient based on the differential mutual information(40–42),

$$IC(x, y) = sign(\rho(x, y))\sqrt{1 - \exp(2I(x, y)} \quad (1)$$

where ρ is the correlation coefficient, x is the oncogenic activation profile, and y is the genomic feature. The sign of the correlation coefficient provides directionality to the metric. The I(x,y) is the differential mutual information between x and y computed using kernel density estimation.

$$I(x,y) = \int\int p(x|y)\log\frac{p(x,y)}{p(x)p(y)}dxdy \quad (2)$$

Where p(x), and p(y) are p(x, y) the joint and marginal probability densities. This type of feature selection process has been used in many of our studies.(43–52)

In order to characterize pathway enrichment, we used our single-sample GSEA (Gene Set Enrichment Analysis) algorithm(53) with gene sets from MSigDB (*Molecular Signatures Database*(33,34)), including recently-added subcollections of oncogenic and hallmark gene sets.(54) This is also the method we use to produce the profiles of pathways in the heatmap of Figure 1.

Onco-GPS components were characterized by matching individual mRNA gene and pathway profiles against the per-sample NMF component amplitudes using the Information Coefficient This was also done with *KIT* mRNA expression in order to investigate its relationship with e.g. stemness pathways.

Statistical Analysis

All statistical analysis was performed using GraphPad Prism 7 (GraphPad Software, La Jolla, CA). Data are reported as means ± standard deviation (SD). Comparisons between controls and experimental groups were analyzed for significance by the Student's t-test (2-tailed) or Mann-Whitney test. Statistical significance was accepted at the 5% level ($P \leq 0.05$). Correction for multiple comparisons was performed when appropriate.

Results

IM increases expression of stem markers in human GIST

We performed GSEA on 18 matched GISTs comparing pre- and post-neoadjuvant IM treatment (RTOG S0132).(28) Post-IM samples had reduced *KIT* (P=0.0002) and *ETV1* (P<0.001) mRNA expression, as well as upregulation of known gene signatures associated with GIST tumorigenesis and IM-resistance. Additionally, we detected activation of several hallmark cancer pathways including "cancer stem cell", NF-κB, PDGFRA, and AXL signaling gene signatures (Fig. 1A). Transcript expression of two stem-associated transcription factors (SATFs), *OCT4* (P<0.05) and *NANOG* (P<0.05), showed induction after treatment with IM while *KIT* expression was suppressed (P<0.001) (Fig. 1B). Enrichment of cancer stem cell gene profiles represented a novel putative mechanism of IM-resistance. We then attempted to confirm this finding using established GIST cell lines. Tumorsphere formation has been associated with cancer "stemness" and can signify enrichment of cancer stem cells.(55) GIST-T1 tumorspheres were treated with imatinib (10 nM) for 72 hours and RT-qPCR was performed. We observed marked induction of SATFs including *OCT4* (8.1-fold, P<0.001) and *NANOG* (12.0-fold, P<0.001) (Fig. 1C). While IM treatment decreased KIT protein (0.41-fold, P=0.048), it induced OCT4 (4.5-fold, P=0.015) and NANOG (2.9-fold, P=0.035) proteins in GIST-T1 tumorspheres (Fig. 1C; Supplementary Fig. 1A). These results were confirmed by immunofluorescence (IF) microscopy. GIST-T1 grown as tumorspheres led to detectable OCT4 and NANOG proteins

as shown in DMSO panels. Treatment of GIST-T1 tumorspheres with imatinib (100 nM) further promoted a subpopulation of cells that highly expressed OCT4 and NANOG (Fig. 1D; Supplementary Fig. 1B). We also identified a similar pattern of scattered expression of SATFs in resected *KIT* exon 11 mutant human GIST imatinib therapy but not in the untreated *KIT* exon 11 mutant GIST (Fig. 1E; Supplementary Fig. 1C). Co-expression of OCT4 and NANOG was observed in the GIST tissues (detected by yellow color in Merge panels).

Treatment naïve GIST cells have properties of "stemness"

In addition to tumorsphere models, we evaluated aldehyde dehydrogenase (ALDH) function, which is an established marker of cell stemness.(56) The GIST882 cell line was found to have a high proportion of $ALDH^{high}$ cells (Fig. 2A). Consistent with aforementioned findings in tumorshpere models, we observed SATF enrichment within the $ALDH^{high}$ subpopulation compared with $ALDH^{low}$ cells (Fig. 2B–C). There was induction of *OCT4* (30.6-fold, P<0.001) and *NANOG* (34.9-fold, P<0.001) transcripts (Fig. 2B), along with the induction of OCT4 (21.5-fold, P=0.041) and NANOG (58.0-fold, P=0.025) proteins (Fig. 2C). Importantly, such $ALDH^{high}$ cells were also detected in primary human GISTs bearing *KIT* exon 11 mutations: GIST#3, *OCT4* (1.9-fold, P<0.05) and *NANOG* (2.3-fold, P<0.01); and GIST#4, *OCT4* (4.1-fold, P<0.001) and *NANOG* (2.3-fold, P<0.05) (Fig. 2D–E). Taken together, putative GIST stem-like cells exist and can be further enriched in 3D culture, as well as in sorted $ALDH^{high}$ subpopulation.

KIT^{low} GIST cells are stem cell-like

As previously reported, GIST CSCs may represent a KIT^{low} population in mice.(24) We next aimed to isolate and study the functional properties of human KIT^{low} cells. We first evaluated the expression of SATFs in KIT^{low} compared to KIT^{high} cells using RT-qPCR.(57) GIST882 KIT^{low} cells had higher expression of *OCT4* (1.6-fold, P=0.0033) and *NANOG* (1.9-fold, P=0.0046) (Fig. 3A). Next, we compared the colony forming potential of single-cell KIT^{low} versus KIT^{high} cells to evaluate their self-renewal proliferation capability. FACS-sorted $KIT^{high}CD34^{+}$ and $KIT^{low}CD34^{+}$ GIST882 were sorted into single cells per well and cultured for 5 weeks and then analyzed for viable cell population. KIT^{low} cells had a higher proliferation potential than KIT^{high} cells (P<0.05) (Fig. 3B). We next analyzed the cell cycle states of KIT^{low} and KIT^{high} cells. GIST-T1 and GIST882 cells showed that KIT^{low} cells had marked enrichment in G0-G1 cells compared to KIT^{high} cells (P<0.001). Importantly, the ratio of KIT^{low} to KIT^{high} cells was unchanged following cell cycle arrest suggesting that KIT expression is not driven by cell cycle state (Supplemental Fig. 2). KIT^{low} cells progressed through the cell cycle, but had a lower proportion of cells arrested at G2/M compared to KIT^{high} cells (P<0.001) in GIST-T1 and GIST882 cells. The proportion of cells in cell cycle states differed between GIST-T1 and GIST882 because the former has a doubling time of 12 hours while the latter doubling time is 24-36 hours. (Fig. 3C). Another hallmark of cancer stem cells is the ability to self-renew and differentiate into mature progeny. We tested the capacity for diffentiation of FACS-sorted KIT^{low} cells to give rise to KIT^{high} cells. FACS-sorted $KIT^{low}CD34^{+}$ GIST882 cells were isolated and cultured for 5 days followed by FCM analyses. KIT^{low} cells recapitulated the original cellular composition of the parental GIST882 cell line although the proportion of KIT^{low}

cells remained higher (Fig. 3D). To examine the proliferative potential of KIT^{low} cells at the tissue level, multiplexing IF was performed in IM-treated GIST using antibodies against KIT, NANOG, and Ki-67. (Fig. 3E). We detected tumor foci containing KIT^{low} cells with co-expression of NANOG and Ki-67. This supports our *in vitro* results in human tumor samples: stem cell-like KIT^{low} cells in GIST have a higher proliferative potential. Taken together, these findings support the notion that KIT^{low} cells have stem-like properties given their capacity to self-renew, differentiate and proliferate.

TKI treatment enriches for KIT^{low} GIST cells

Gene expression analysis of matched samples pre- and post-IM treatment (Fig. 1) showed reduced *KIT* expression in imatinib treated tumors. Next, we examined the proportion of KIT^{low} cells before and after imatinib treatment. IM treatment resulted in an increase in the population of KIT^{low} cells (25.1% increase, P=0.01) and concomitant decrease in KIT^{high} cells (25% decrease, P=0.008) (Fig. 4A). We then tested the sensitivity of sorted cells to imatinib treatment. KIT^{high} cells were sensitive to imatinib treatment across a range of drug doses as compared to KIT^{low} cells that demonstrated relative imatinib resistance, even at high drug doses (Fig. 4B). Lastly, we examined early changes in the proportion of KIT^{low} and KIT^{high} cells in order to determine whether KIT^{low} cell enrichment is a consequence of receptor downregulation or proliferation of the KIT^{low} subpopulation (Fig. 4C–D). KIT^{high} cells from GIST882 pre-treated with short duration, high dose of imatinib had stable viability between 1 to 6 hours (1-hr and 3-hr, Supplemental Fig. 3) whereas significant cell death started at 24-hr post-IM. In contrast, the KIT^{low} population was increased resulting from two events: 1) KIT protein was slightly down modulated by 6-hrs post-IM and then up to 24 hours **(**1-hr and 3-hr, Supplemental Fig. 3); 2) cell death of KIT^{high} cells began at the 24-hr time point leading to an additional enrichment of the KIT^{low} population (Fig. 4C–D). This suggests that KIT^{low} cells primarily represent a cell population insensitive to imatinib and there are two potential mechanisms, namely receptor downregulation and enrichment of insensitive cells, for imatinib resistance.

To address the stem-like proliferative potential of KIT^{low} cells *in vivo*, we utilized a spleen-to-liver metastasis mouse model as we have previously reported.(58) mCherry-labeled T1 cells after IM treatment were sorted into KIT^{high} and KIT^{low} cells. Equal cell numbers from each sub-population were injected into the spleens of nude mice (n = 3 per group) and liver metastases were evaluated (Fig. 4E–F; Supplementary Fig. 4). KIT^{low} cells show engraftment potential in this metastatic GIST animal model. Taken together, our findings indicate that imatinib treatment enriches KIT^{low} cells have higher proliferative potential *in vitro* and *in vivo*.

KIT^{low} primary tumors have distinct pathway activation

KIT^{low} cells are present in genetically diverse forms of GIST. To better understand pathway activation that predominates within the KIT^{low} subpopulation, we utilized a bioinformatic approach. In this analysis framework, GIST samples are used to define top oncogenic states and the top transcriptional component pathways that are statistically significant or near significant.(32) The map defines the top 5 oncogenic states and the top 5 transcriptional component pathways in GIST (Supplementary Fig. 5). In an unsupervised manner, the map

naturally separates states based on *KIT* expression (Fig. 5). Interrogating KIT^{low} samples revealed 2 distinct oncogenic states. One state was of particular interest (circled), which is associated with stem cell pathways, Gas6/AXL (transcript expression) and NF-κB gene sets. This agnostic data-driven approach serves as an encouraging validation of the *in vitro* cell line and primary tumor analysis that SATF activation occurs in KIT^{low} cells. Furthermore, the value of the Onco-GPS map is to understand parallel pathway activation within a given oncogenic state. We noted that AXL and NF-κB were associated with a KIT^{low} state. This is supported by enrichment of NF-κB (gene sets) and AXL receptor (transcripts) in the IM-treated tumors (GEO dataset GSE15966(28)) (Fig. 1A). Therefore, these pathways may represent novel targets for inhibition of KIT^{low} GIST cells.

NF-κB and GAS6/AXL inhibition augments imatinib toxicity

We next tested the *in vitro* effect of TKI treatment in GIST cell lines. As demonstrated previously, IM treatment results in enrichment of resistant KIT^{low} cells. GIST882 cells treated for 3 days with IM (300 nM) resulted in 46% cell viability as compared to control treatment (P<0.001, Fig. 6A). Cells were then retreated with imatinib for an additional 3 days or switched to DMSO for a total of 6-day treatment. Subsequent treatment with DMSO resulted in expected cell recovery. However, additional treatment with imatinib had limited additional toxicity with a final cell viability of 32%. Based on our prior evidence, we hypothesized that the plateau in cytotoxicity (between 3- and 6-day IM treatment) is determined by the KIT^{low} subpopulation. We next aimed to apply the insights gleaned through the Onco-GPS map to drug pathways that may target KIT^{low} cells. The Onco-GPS map revealed enrichment in TAM receptors (Tyro3, AXL, and MerTK) in KIT^{low}, which are known to mediate TKI resistance in several cancer types.(59) Additionally, NF-κB is a well-established regulator of stemness and drug resistance.(60) To test these hypotheses, we utilized inhibitors for TAM receptors (R428, bemcentinib/BEM(61)) and NF-κB (bardoxolone/BARD(62)). We tested cytotoxicity of unsorted cells after pretreatment with imatinib (185 nM, for 72 hours) to enrich KIT^{low} cells for subsequent treatments. Imatinib sensitized cells to BEM (1 μM, 70%, P<0.001), and BARD (1 μM, 73%, P<0.001) (Fig. 6B). In addition, combination treatment with imatinib and either inhibitor was more effective than imatinib treatment alone, exerting killing up to 85% as compared with controls **(**P<0.05, Fig. 6B). Similar effects were observed in GIST-T1 cells. More specifically, T1 cells treated for 3 days with IM (20 nM) resulted in 44% cell viability as compared to control treatment (P<0.001, Fig. 6C). Imatinib sensitized T1 cells to BEM (1 μM, 82%, P<0.001) and BARD (1 μM, 62%, P<0.001) (Fig. 6D). Combination of imatinib with either BEM or BARD was more potent than imatinib alone (P<0.001, Fig. 6D). We next sought to access the change of AXL and NF-κB expression when treated with BEM and BARD inhibitors, respectively. Our data showed that a decrease in NF-kB p65 phosphorylation level was detected as early as 60 minutes when inhibited with BARD (Fig. 6E). Inhibition of AXL phosphorylation by BEM treatment was detected as early as 30 minutes (Fig. 6F). Taken together, these data indicate that IM-resistant KIT^{low} GIST cells are a targetable compartment, and that inhibition of TAM- and NF-κB pathways alone or in combination with TKI can serve as platforms for future studies.

Discussion

Imatinib (IM) activity in gastrointestinal stromal tumor serves as a paradigm for targeted therapy in solid organ malignancies. However, IM does not cure GIST and a majority of patients either develop resistance on therapy, or experience disease recurrence after discontinuation of therapy. Failure of KIT targeted therapies prompted us to hypothesize that a KIT-insensitive subpopulation may serve as a mechanism of disease persistence. In this study, we find that KIT^{low} cells are a distinct subpopulation in human GIST, which have intrinsic (i.e., *de novo* or primary) IM-resistance. Moreover, TKI treatment induces enrichment of this KIT^{low} cellular subpopulation, which expresses stem-associated transcription factors and has several functional properties of *bona fide* cancer stem cells *in vitro* and *in vivo*. To further characterize the KIT^{low} phenotype, we employed a data-driven integrative bioinformatic approach which identified Gas6/AXL and the NF-κB pathway as putative novel therapeutic targets *in vitro*. Together, these data suggest that KIT^{low} cells may function as a targetable cellular compartment in GIST that is a source of disease persistence despite molecularly matched therapy for *KIT* oncogene driven disease.

The role of cancer stem cells (CSCs) in GIST has been poorly understood. Characterization of GIST CSCs has been partly derailed by the observation that well established markers of CSCs (e.g., CD44 and CD133) are ubiquitously expressed on GIST cells.(23) Additionally, KIT/CD117 is the stem cell factor receptor (SCFR) and has been proposed as the source of drug resistance, disease recurrence, and metastasis in many other tumor types.(63,64) In the absence of established surface markers, several studies have interrogated alternate candidates for markers of GIST CSCs. BMI1, TERT and KLF4 were found to be preferentially expressed in GISTs, and expression of BMI1 was found to correlate with advanced disease.(65) Moreover, Nestin, or neuroectodermal stem cell marker, expression has also been reported as a marker of aggressive forms of GIST.(66) In the current study, we find that OCT4 and NANOG are previously unappreciated stem cell associated transcription factors (SATFs) that were upregulated following TKI treatment and overexpressed in $ALDH^{high}$ and KIT^{low} GIST cells, which both have selected hallmarks of CSC-like cells.

Although these associations are valuable, the first mechanistic insight into the role of CSCs in GIST was described in a mouse model of progenitor ICCs.(24) Bardsley *et al.* discovered an ICC progenitor in the gastric wall of mice with properties of stem cells including self-renewal and the ability to differentiate into mature ICCs. A cell line derived from this ICC progenitor demonstrated spontaneous transformation resulting in the formation of GIST-like tumors. Importantly, this ICC progenitor was noted to have low KIT expression compared to its mature ICC counterpart. Here, we find that KIT^{low} cells are a distinct cellular subpopulation within human GISTs. These cells are quiescent, but have greater replicative capacity and superior colony-forming potential than KIT^{high} cells. Additionally, isolated and cultured KIT^{low} cells give rise to KIT^{high} cells. Moreover, imatinib treatment preferentially enriches KIT^{low} cells while having a cytotoxic effect on KIT^{high} cells. These results suggest that KIT^{low} cells have stem-like properties, and may represent a reservoir for disease persistence following TKI therapy. This model mirrors an established mechanism of CML disease persistence in which CML stem progenitors have been shown to be quiescent, stem-like cells that exhibit imatinib resistance.(67)

The notion that some GIST lack KIT expression is known and these KIT-negative tumors were found to harbor primarily *PDGFRA* mutations.(68) In a recent paper, Tu *et al.* profiled tyrosine kinases that were differentially activated in IM-resistant cell lines of KIT-negative GIST.(69) They found that EGFR, AXL, EPHA2 and FAK were active in KIT-negative cell lines. Interestingly, AXL knockdown and pathway inhibition was found to be cytotoxic in an IM-resistant GIST line. AXL has also been previously shown to be important in imatinib-resistant GIST.(70,71) In the current study, we utilized a bioinformatic approach to identify co-functioning pathways within a KIT^{low}, stem cell associated oncogenic state. We confirmed that Gas6/AXL and other TAM receptors (Tyro3 and MerTK) were associated with this state. AXL is an attractive target as it has also been previously reported to increase tumorigenicity of breast CSCs resulting in decreased breast CSC chemosensitivity.(72) Increased expression of AXL also accounts for TKI resistance in *EGFR*-mutant non-small cell lung cancer,(73) pancreatic cancer metastases,(74) and melanoma.(47,75) In addition to the prior reports in GIST, we now find that AXL inhibition augments imatinib cytotoxicity presumably by targeting the KIT^{low} compartment. This result was observed in imatinib-naïve cells compared to imatinib-resistant cell lines as shown in prior reports.(69,70) The Onco-GPS bioinformatic analysis also suggested that NF-κB is active in KIT^{low} cells. NF-κB has been previously implicated in GIST tumorigenesis through an autoregulatory loop or recruitment of tumor-associated macrophages.(76,77) Here, we found that the addition of NF-κB inhibition to imatinib resulted in augmented cell killing over IM-treatment alone. Thus, our findings provide new evidence for therapeutic targets in a rare subpopulation of GIST that is imatinib-resistant in the absence of imatinib selection pressure.

This study has several limitations. First, KIT^{low} cells are a rare cell subpopulation. FACS-isolated KIT^{low} cells “differentiate” quickly, which poses technical challenges to studying this cell population in downstream experiments. We addressed this by enriching the proportion of KIT^{low} cells with imatinib pretreatment prior to FACS, which also mimics patient treatment schema. Indeed, our data supported the notion that TKI-resistant cells with stem-like characteristics are responsible for disease recurrence. However, an immortalized cell line would be a valuable resource to study this cell population. Additionally, negative marker selection is a suboptimal method of cellular sorting. We attempted several methods of transcriptomic and proteomic screening KIT^{low} cells for over 240 surface markers (Supplemental Table 3). However, we were not able to identify a unique positive selection marker for the subpopulation. We addressed this limitation by performing a rigid methodology of fluorescence minus one (FMO) controls within our FACS protocol that enabled reproducible isolation of the KIT^{low} subpopulation, which was capable of complementary analyses.

Despite the success of IM in GIST therapy, disease persistence remains an unaddressed challenge. Here, we report that KIT^{low} cells are stem-like cells within human GISTs that have primary IM resistance. These KIT^{low} cells also possess distinct pathway activation that can be targeted to eradicate this IM-resistant cellular compartment. Our findings support the role of combinatorial therapeutic approaches to overcome drug resistance or to treat disease persistence in GIST.

Supplementary Material

Refer to Web version on PubMed Central for supplementary material.

Conflict of interest:

J.K.S receives research funding from Amgen Pharmaceuticals and Foundation Medicine, consultant fees from Deciphera, speaker's fees from Deciphera, Foundation Medicine, La-Hoffman Roche, Merck, MJH Life Sciences, QED Therapeutics, and has stock in Personalis. These disclosures had no impact on any of the work presented in this manuscript. There are no conflicts of interest to declare by the remaining authors.

Financial Support:

We appreciate funding support from the Surgical Society of the Alimentary Tract (SSAT) Mentored Research Award (S.B.) and NIH T32 CA121938 Cancer Therapeutics (CT2) Training Fellowship (S.B.). In addition, we appreciate funding support from Hope for a Cure Foundation (J.K.S.), The Life Raft Group (J.K.S.), Kristen Ann Carr Fund (J.K.S.), Lighting the Path Forward for GIST Cancer Research (J.K.S.), The David Foundation (J.K.S.), Pedal the Cause (J.K.S., R.W-R.), NIH K08 CA168999 (J.K.S.), NIH R01 CA226803 (J.K.S.), FDA R01 FD006334 (J.K.S.), R01CA226803 (P.T), U01CA217885 (P.T, J.M., H.Y., S.T.), U24CA194107 (J.M., P.T), U24 CA220341 (JM, PT), R01 GM074024 (JM, PT), U24 CA248457 (J.M., P.T.), P30 CA023100 (P.T. HY, ST), R01HG009285 (P.T), R01DE026870 (P.T), U01DE028227 (P.T), U54CA209891 (P.T) and T15LM011271 (ATW).

References

1. Ma GL, Murphy JD, Martinez ME, Sicklick JK. Epidemiology of gastrointestinal stromal tumors in the era of histology codes: results of a population-based study. Cancer Epidemiol Biomarkers Prev2015;24(1):298–302 doi 10.1158/1055-9965.EPI-14-1002. [PubMed: 25277795]
2. Joensuu H, Vehtari A, Riihimaki J, Nishida T, Steigen SE, Brabec P, et al. Risk of recurrence of gastrointestinal stromal tumour after surgery: an analysis of pooled population-based cohorts. Lancet Oncol2012;13(3):265–74 doi 10.1016/S1470-2045(11)70299-6. [PubMed: 22153892]
3. Dematteo RP, Ballman KV, Antonescu CR, Maki RG, Pisters PW, Demetri GD, et al. Adjuvant imatinib mesylate after resection of localised, primary gastrointestinal stromal tumour: a randomised, double-blind, placebo-controlled trial. Lancet2009;373(9669):1097–104 doi 10.1016/S0140-6736(09)60500-6. [PubMed: 19303137]
4. Joensuu H, Eriksson M, Sundby Hall K, Hartmann JT, Pink D, Schutte J, et al. One vs three years of adjuvant imatinib for operable gastrointestinal stromal tumor: a randomized trial. JAMA2012;307(12):1265–72 doi 10.1001/jama.2012.347. [PubMed: 22453568]
5. Le Cesne A, Ray-Coquard I, Bui BN, Adenis A, Rios M, Bertucci F, et al. Discontinuation of imatinib in patients with advanced gastrointestinal stromal tumours after 3 years of treatment: an open-label multicentre randomised phase 3 trial. Lancet Oncol2010;11(10):942–9 doi 10.1016/S1470-2045(10)70222-9. [PubMed: 20864406]
6. Reichardt P, Demetri GD, Gelderblom H, Rutkowski P, Im SA, Gupta S, et al. Correlation of KIT and PDGFRA mutational status with clinical benefit in patients with gastrointestinal stromal tumor treated with sunitinib in a worldwide treatment-use trial. BMC Cancer2016;16:22 doi 10.1186/s12885-016-2051-5. [PubMed: 26772734]
7. Ben-Ami E, Barysauskas CM, von Mehren M, Heinrich MC, Corless CL, Butrynski JE, et al. Long-term follow-up results of the multicenter phase II trial of regorafenib in patients with metastatic and/or unresectable GI stromal tumor after failure of standard tyrosine kinase inhibitor therapy. Ann Oncol2016;27(9):1794–9 doi 10.1093/annonc/mdw228. [PubMed: 27371698]
8. Wardelmann E, Thomas N, Merkelbach-Bruse S, Pauls K, Speidel N, Buttner R, et al. Acquired resistance to imatinib in gastrointestinal stromal tumours caused by multiple KIT mutations. Lancet Oncol2005;6(4):249–51 doi 10.1016/S1470-2045(05)70097-8. [PubMed: 15811621]
9. Alkhuziem M, Burgoyne AM, Fanta PT, Tang CM, Sicklick JK. The Call of "The Wild"-Type GIST: It's Time for Domestication. J Natl Compr Canc Netw2017;15(5):551–4. [PubMed: 28476734]
10. Corless CL, Barnett CM, Heinrich MC. Gastrointestinal stromal tumours: origin and molecular oncology. Nat Rev Cancer2011;11(12):865–78 doi 10.1038/nrc3143. [PubMed: 22089421]

11. Burgoyne AM, Somaiah N, Sicklick JK. Gastrointestinal Stromal Tumors in the Setting of Multiple Tumor Syndromes. Current Opinion in Oncology2014:In Press.
12. Heinrich MC, Jones RL, von Mehren M, Schoffski P, Serrano C, Kang YK, et al. Avapritinib in advanced PDGFRA D842V-mutant gastrointestinal stromal tumour (NAVIGATOR): a multicentre, open-label, phase 1 trial. Lancet Oncol2020;21(7):935–46 doi 10.1016/S1470-2045(20)30269-2. [PubMed: 32615108]
13. Rubin BP, Heinrich MC, Corless CL. Gastrointestinal stromal tumour. Lancet2007;369(9574):1731–41 doi 10.1016/S0140-6736(07)60780-6. [PubMed: 17512858]
14. Liegl-Atzwanger B, Fletcher JA, Fletcher CD. Gastrointestinal stromal tumors. Virchows Arch2010;456(2):111–27 doi 10.1007/s00428-010-0891-y. [PubMed: 20165865]
15. Agaram NP, Wong GC, Guo T, Maki RG, Singer S, Dematteo RP, et al. Novel V600E BRAF mutations in imatinib-naive and imatinib-resistant gastrointestinal stromal tumors. Genes Chromosomes Cancer2008;47(10):853–9 doi 10.1002/gcc.20589. [PubMed: 18615679]
16. Shi E, Chmielecki J, Tang CM, Wang K, Heinrich MC, Kang G, et al. FGFR1 and NTRK3 actionable alterations in “Wild-Type” gastrointestinal stromal tumors. J Transl Med2016;14(1):339 doi 10.1186/s12967-016-1075-6. [PubMed: 27974047]
17. Brenca M, Rossi S, Polano M, Gasparotto D, Zanatta L, Racanelli D, et al. Transcriptome sequencing identifies ETV6-NTRK3 as a gene fusion involved in GIST. J Pathol2015 doi 10.1002/path.4677.
18. Hechtman JF, Zehir A, Mitchell T, Borsu L, Singer S, Tap W, et al. Novel oncogene and tumor suppressor mutations in KIT and PDGFRA wild type gastrointestinal stromal tumors revealed by next generation sequencing. Genes Chromosomes Cancer2015;54(3):177–84 doi 10.1002/gcc.22230. [PubMed: 25427437]
19. Seidal T, Edvardsson H. Expression of c-kit (CD117) and Ki67 provides information about the possible cell of origin and clinical course of gastrointestinal stromal tumours. Histopathology1999;34(5):416–24. [PubMed: 10231416]
20. Sircar K, Hewlett BR, Huizinga JD, Chorneyko K, Berezin I, Riddell RH. Interstitial cells of Cajal as precursors of gastrointestinal stromal tumors. Am J Surg Pathol1999;23(4):377–89. [PubMed: 10199467]
21. Wang L, Vargas H, French SW. Cellular origin of gastrointestinal stromal tumors: a study of 27 cases. Arch Pathol Lab Med2000;124(10):1471–5. [PubMed: 11035578]
22. Beadling C, Patterson J, Justusson E, Nelson D, Pantaleo MA, Hornick JL, et al. Gene expression of the IGF pathway family distinguishes subsets of gastrointestinal stromal tumors wild type for KIT and PDGFRA. Cancer Med2013;2(1):21–31 doi 10.1002/cam4.57. [PubMed: 24133624]
23. Chen J, Guo T, Zhang L, Qin LX, Singer S, Maki RG, et al. CD133 and CD44 are universally overexpressed in GIST and do not represent cancer stem cell markers. Genes Chromosomes Cancer2011 doi 10.1002/gcc.20942.
24. Bardsley MR, Horvath VJ, Asuzu DT, Lorincz A, Redelman D, Hayashi Y, et al. Kitlow stem cells cause resistance to Kit/platelet-derived growth factor alpha inhibitors in murine gastrointestinal stromal tumors. Gastroenterology2010;139(3):942–52 doi 10.1053/j.gastro.2010.05.083. [PubMed: 20621681]
25. Taguchi T, Sonobe H, Toyonaga S, Yamasaki I, Shuin T, Takano A, et al. Conventional and molecular cytogenetic characterization of a new human cell line, GIST-T1, established from gastrointestinal stromal tumor. Lab Invest2002;82(5):663–5. [PubMed: 12004007]
26. Tuveson DA, Willis NA, Jacks T, Griffin JD, Singer S, Fletcher CD, et al. STI571 inactivation of the gastrointestinal stromal tumor c-KIT oncoprotein: biological and clinical implications. Oncogene2001;20(36):5054–8 doi 10.1038/sj.onc.1204704. [PubMed: 11526490]
27. Sicklick JK, Li YX, Jayaraman A, Kannangai R, Qi Y, Vivekanandan P, et al. Dysregulation of the Hedgehog pathway in human hepatocarcinogenesis. Carcinogenesis2006;27(4):748–57 doi 10.1093/carcin/bgi292. [PubMed: 16339184]
28. Rink L, Skorobogatko Y, Kossenkov AV, Belinsky MG, Pajak T, Heinrich MC, et al. Gene expression signatures and response to imatinib mesylate in gastrointestinal stromal tumor. Mol Cancer Ther2009;8(8):2172–82 doi 1535-7163.MCT-09-0193 [pii] 10.1158/1535-7163.MCT-09-0193. [PubMed: 19671739]

29. Subramanian A, Tamayo P, Mootha VK, Mukherjee S, Ebert BL, Gillette MA, et al. Gene set enrichment analysis: a knowledge-based approach for interpreting genome-wide expression profiles. Proc Natl Acad Sci U S A2005;102(43):15545–50 doi 10.1073/pnas.0506580102. [PubMed: 16199517]
30. Mootha VK, Lindgren CM, Eriksson KF, Subramanian A, Sihag S, Lehar J, et al. PGC-1alpha-responsive genes involved in oxidative phosphorylation are coordinately downregulated in human diabetes. Nat Genet2003;34(3):267–73 doi 10.1038/ng1180. [PubMed: 12808457]
31. Vitiello GA, Bowler TG, Liu M, Medina BD, Zhang JQ, Param NJ, et al. Differential immune profiles distinguish the mutational subtypes of gastrointestinal stromal tumor. J Clin Invest2019;129(5):1863–77 doi 10.1172/JCI124108. [PubMed: 30762585]
32. Kim JW, Abudayyeh OO, Yeerna H, Yeang CH, Stewart M, Jenkins RW, et al. Decomposing Oncogenic Transcriptional Signatures to Generate Maps of Divergent Cellular States. Cell Syst2017;5(2):105–18 e9 doi 10.1016/j.cels.2017.08.002. [PubMed: 28837809]
33. Liberzon A, Subramanian A, Pinchback R, Thorvaldsdottir H, Tamayo P, Mesirov JP. Molecular signatures database (MSigDB) 3.0. Bioinformatics2011;27(12):1739–40 doi 10.1093/bioinformatics/btr260. [PubMed: 21546393]
34. Liberzon AA description of the Molecular Signatures Database (MSigDB) Web site. Methods Mol Biol2014;1150:153–60 doi 10.1007/978-1-4939-0512-6_9. [PubMed: 24743996]
35. Ostrowski J, Polkowski M, Paziewska A, Skrzypczak M, Goryca K, Rubel T, et al. Functional features of gene expression profiles differentiating gastrointestinal stromal tumours according to KIT mutations and expression. BMC Cancer2009;9:413 doi 1471-2407-9-413 [pii] 10.1186/1471-2407-9-413. [PubMed: 19943934]
36. Astolfi A, Nannini M, Pantaleo MA, Di Battista M, Heinrich MC, Santini D, et al. A molecular portrait of gastrointestinal stromal tumors: an integrative analysis of gene expression profiling and high-resolution genomic copy number. Lab Invest2010;90(9):1285–94 doi labinvest2010110 [pii] 10.1038/labinvest.2010.110. [PubMed: 20548289]
37. Edgar R, Domrachev M, Lash AE. Gene Expression Omnibus: NCBI gene expression and hybridization array data repository. Nucleic Acids Res2002;30(1):207–10 doi 10.1093/nar/30.1.207. [PubMed: 11752295]
38. Kang HJ, Nam SW, Kim H, Rhee H, Kim NG, Kim H, et al. Correlation of KIT and platelet-derived growth factor receptor alpha mutations with gene activation and expression profiles in gastrointestinal stromal tumors. Oncogene2005;24(6):1066–74 doi 10.1038/sj.onc.1208358. [PubMed: 15690055]
39. Kannan R, Ballard G, Park H. A high-performance parallel algorithm for nonnegative matrix factorization. Proceedings of the 21st ACM SIGPLAN Symposium on Principles and Practice of Parallel Programming. Barcelona, Spain: Association for Computing Machinery; 2016. p Article 9.
40. Kim JW, Botvinnik OB, Abudayyeh O, Birger C, Rosenbluh J, Shrestha Y, et al. Characterizing genomic alterations in cancer by complementary functional associations. Nat Biotechnol2016;34(5):539–46 doi 10.1038/nbt.3527. [PubMed: 27088724]
41. Joe HRelative Entropy Measures of Multivariate Dependence. Journal of the American Statistical Association1989;84(405):157–64 doi 10.1080/01621459.1989.10478751.
42. Linfoot EH. An informational measure of correlation. Information and Control1957;1(1):85–9 doi 10.1016/S0019-9958(57)90116-X.
43. Cowley GS, Weir BA, Vazquez F, Tamayo P, Scott JA, Rusin S, et al. Parallel genome-scale loss of function screens in 216 cancer cell lines for the identification of context-specific genetic dependencies. Sci Data2014;1:140035 doi 10.1038/sdata.2014.35. [PubMed: 25984343]
44. Abazeed ME, Adams DJ, Hurov KE, Tamayo P, Creighton CJ, Sonkin D, et al. Integrative radiogenomic profiling of squamous cell lung cancer. Cancer Res2013;73(20):6289–98 doi 10.1158/0008-5472.CAN-13-1616. [PubMed: 23980093]
45. Stewart ML, Tamayo P, Wilson AJ, Wang S, Chang YM, Kim JW, et al. KRAS Genomic Status Predicts the Sensitivity of Ovarian Cancer Cells to Decitabine. Cancer Res2015;75(14):2897–906 doi 10.1158/0008-5472.CAN-14-2860. [PubMed: 25968887]

46. Wilson FH, Johannessen CM, Piccioni F, Tamayo P, Kim JW, Van Allen EM, et al. A functional landscape of resistance to ALK inhibition in lung cancer. Cancer Cell2015;27(3):397–408 doi 10.1016/j.ccell.2015.02.005. [PubMed: 25759024]
47. Konieczkowski DJ, Johannessen CM, Abudayyeh O, Kim JW, Cooper ZA, Piris A, et al. A melanoma cell state distinction influences sensitivity to MAPK pathway inhibitors. Cancer Discov2014;4(7):816–27 doi 10.1158/2159-8290.CD-13-0424. [PubMed: 24771846]
48. Hanaford AR, Archer TC, Price A, Kahlert UD, Maciaczyk J, Nikkhah G, et al. DiSCoVERing Innovative Therapies for Rare Tumors: Combining Genetically Accurate Disease Models with In Silico Analysis to Identify Novel Therapeutic Targets. Clin Cancer Res2016;22(15):3903–14 doi 10.1158/1078-0432.CCR-15-3011. [PubMed: 27012813]
49. Feng X, Arang N, Rigiracciolo DC, Lee JS, Yeerna H, Wang Z, et al. A Platform of Synthetic Lethal Gene Interaction Networks Reveals that the GNAQ Uveal Melanoma Oncogene Controls the Hippo Pathway through FAK. Cancer Cell2019;35(3):457–72 e5 doi 10.1016/j.ccell.2019.01.009. [PubMed: 30773340]
50. Reilly B, Tanaka TN, Diep D, Yeerna H, Tamayo P, Zhang K, et al. DNA methylation identifies genetically and prognostically distinct subtypes of myelodysplastic syndromes. Blood Adv2019;3(19):2845–58 doi 10.1182/bloodadvances.2019000192. [PubMed: 31582393]
51. Liu C, Sadat SH, Ebisumoto K, Sakai A, Panuganti BA, Ren S, et al. Cannabinoids Promote Progression of HPV-Positive Head and Neck Squamous Cell Carcinoma via p38 MAPK Activation. Clinical cancer research : an official journal of the American Association for Cancer Research2020;26(11):2693–703 doi 10.1158/1078-0432.CCR-18-3301. [PubMed: 31932491]
52. Kim JW, Berrios C, Kim M, Schade AE, Adelmant G, Yeerna H, et al. STRIPAK directs PP2A activity toward MAP4K4 to promote oncogenic transformation of human cells. Elife2020;9 doi 10.7554/eLife.53003.
53. Barbie DA, Tamayo P, Boehm JS, Kim SY, Moody SE, Dunn IF, et al. Systematic RNA interference reveals that oncogenic KRAS-driven cancers require TBK1. Nature2009;462(7269):108–12 doi 10.1038/nature08460. [PubMed: 19847166]
54. Liberzon A, Birger C, Thorvaldsdottir H, Ghandi M, Mesirov JP, Tamayo P. The Molecular Signatures Database (MSigDB) hallmark gene set collection. Cell Syst2015;1(6):417–25 doi 10.1016/j.cels.2015.12.004. [PubMed: 26771021]
55. Chaicharoenaudomrung N, Kunhorm P, Noisa P. Three-dimensional cell culture systems as an in vitro platform for cancer and stem cell modeling. World J Stem Cells2019;11(12):1065–83 doi 10.4252/wjsc.v11.i12.1065. [PubMed: 31875869]
56. Ma I, Allan AL. The role of human aldehyde dehydrogenase in normal and cancer stem cells. Stem Cell Rev Rep2011;7(2):292–306 doi 10.1007/s12015-010-9208-4. [PubMed: 21103958]
57. Yu J, Vodyanik MA, Smuga-Otto K, Antosiewicz-Bourget J, Frane JL, Tian S, et al. Induced pluripotent stem cell lines derived from human somatic cells. Science2007;318(5858):1917–20 doi 10.1126/science.1151526. [PubMed: 18029452]
58. Yoon H, Tang CM, Banerjee S, Yebra M, Noh S, Burgoyne AM, et al. Cancer-associated fibroblast secretion of PDGFC promotes gastrointestinal stromal tumor growth and metastasis. Oncogene2021 doi 10.1038/s41388-021-01685-w.
59. Vouri M, Hafizi S. TAM Receptor Tyrosine Kinases in Cancer Drug Resistance. Cancer Res2017;77(11):2775–8 doi 10.1158/0008-5472.CAN-16-2675. [PubMed: 28526769]
60. Kaltschmidt C, Banz-Jansen C, Benhidjeb T, Beshay M, Forster C, Greiner J, et al. A Role for NF-kappaB in Organ Specific Cancer and Cancer Stem Cells. Cancers (Basel)2019;11(5) doi 10.3390/cancers11050655.
61. Holland SJ, Pan A, Franci C, Hu Y, Chang B, Li W, et al. R428, a selective small molecule inhibitor of Axl kinase, blocks tumor spread and prolongs survival in models of metastatic breast cancer. Cancer Res2010;70(4):1544–54 doi 10.1158/0008-5472.CAN-09-2997. [PubMed: 20145120]
62. Ahmad R, Raina D, Meyer C, Kharbanda S, Kufe D. Triterpenoid CDDO-Me blocks the NF-kappaB pathway by direct inhibition of IKKbeta on Cys-179. J Biol Chem2006;281(47):35764–9 doi 10.1074/jbc.M607160200. [PubMed: 16998237]

63. Foster BM, Zaidi D, Young TR, Mobley ME, Kerr BA. CD117/c-kit in Cancer Stem Cell-Mediated Progression and Therapeutic Resistance. Biomedicines2018;6(1) doi 10.3390/biomedicines6010031.
64. Tomizawa F, Jang MK, Mashima T, Seimiya H. c-KIT regulates stability of cancer stemness in CD44-positive colorectal cancer cells. Biochem Biophys Res Commun2020;527(4):1014–20 doi 10.1016/j.bbrc.2020.05.024. [PubMed: 32439168]
65. Bai C, Liu X, Xu J, Qiu C, Wang R, Zheng J. Expression profiles of stemness genes in gastrointestinal stromal tumor. Hum Pathol2018;76:76–84 doi 10.1016/j.humpath.2018.02.015. [PubMed: 29486292]
66. Yang XH, Wu QL, Yu XB, Xu CX, Ma BF, Zhang XM, et al. Nestin expression in different tumours and its relevance to malignant grade. J Clin Pathol2008;61(4):467–73 doi jcp.2007.047605 [pii] 10.1136/jcp.2007.047605. [PubMed: 17873113]
67. Corbin AS, Agarwal A, Loriaux M, Cortes J, Deininger MW, Druker BJ. Human chronic myeloid leukemia stem cells are insensitive to imatinib despite inhibition of BCR-ABL activity. J Clin Invest2011;121(1):396–409 doi 10.1172/JCI35721. [PubMed: 21157039]
68. Medeiros F, Corless CL, Duensing A, Hornick JL, Oliveira AM, Heinrich MC, et al. KIT-negative gastrointestinal stromal tumors: proof of concept and therapeutic implications. Am J Surg Pathol2004;28(7):889–94 doi 00000478-200407000-00007 [pii]. [PubMed: 15223958]
69. Tu Y, Zuo R, Ni N, Eilers G, Wu D, Pei Y, et al. Activated tyrosine kinases in gastrointestinal stromal tumor with loss of KIT oncoprotein expression. Cell cycle (Georgetown, Tex)2018;17(23):2577–92 doi 10.1080/15384101.2018.1553335.
70. Mahadevan D, Cooke L, Riley C, Swart R, Simons B, Della Croce K, et al. A novel tyrosine kinase switch is a mechanism of imatinib resistance in gastrointestinal stromal tumors. Oncogene2007;26(27):3909–19 doi 1210173 [pii] 10.1038/sj.onc.1210173. [PubMed: 17325667]
71. Mahadevan D, Theiss N, Morales C, Stejskal AE, Cooke LS, Zhu M, et al. Novel receptor tyrosine kinase targeted combination therapies for imatinib-resistant gastrointestinal stromal tumors (GIST). Oncotarget2015;6(4):1954–66 doi 10.18632/oncotarget.3021. [PubMed: 25557174]
72. Asiedu MK, Beauchamp-Perez FD, Ingle JN, Behrens MD, Radisky DC, Knutson KL. AXL induces epithelial-to-mesenchymal transition and regulates the function of breast cancer stem cells. Oncogene2014;33(10):1316–24 doi 10.1038/onc.2013.57. [PubMed: 23474758]
73. Zhang Z, Lee JC, Lin L, Olivas V, Au V, LaFramboise T, et al. Activation of the AXL kinase causes resistance to EGFR-targeted therapy in lung cancer. Nat Genet2012;44(8):852–60 doi 10.1038/ng.2330. [PubMed: 22751098]
74. Kirane A, Ludwig KF, Sorrelle N, Haaland G, Sandal T, Ranaweera R, et al. Warfarin Blocks Gas6-Mediated Axl Activation Required for Pancreatic Cancer Epithelial Plasticity and Metastasis. Cancer Res2015;75(18):3699–705 doi 10.1158/0008-5472.CAN-14-2887-T. [PubMed: 26206560]
75. Wood KC, Konieczkowski DJ, Johannessen CM, Boehm JS, Tamayo P, Botvinnik OB, et al. MicroSCALE screening reveals genetic modifiers of therapeutic response in melanoma. Sci Signal2012;5(224):rs4 doi 10.1126/scisignal.2002612. [PubMed: 22589389]
76. Hsueh YS, Chang HH, Shan YS, Sun HS, Fletcher JA, Li CF, et al. Nuclear KIT induces a NFKBIB-RELA-KIT autoregulatory loop in imatinib-resistant gastrointestinal stromal tumors. Oncogene2019;38(38):6550–65 doi 10.1038/s41388-019-0900-9. [PubMed: 31363162]
77. Mu J, Sun P, Ma Z, Sun P. BRD4 promotes tumor progression and NF-kappaB/CCL2-dependent tumor-associated macrophage recruitment in GIST. Cell Death Dis2019;10(12):935 doi 10.1038/s41419-019-2170-4. [PubMed: 31819043]
78. Eisenberg BL, Harris J, Blanke CD, Demetri GD, Heinrich MC, Watson JC, et al. Phase II trial of neoadjuvant/adjuvant imatinib mesylate (IM) for advanced primary and metastatic/recurrent operable gastrointestinal stromal tumor (GIST): early results of RTOG 0132/ACRIN 6665. J Surg Oncol2009;99(1):42–7 doi 10.1002/jso.21160. [PubMed: 18942073]

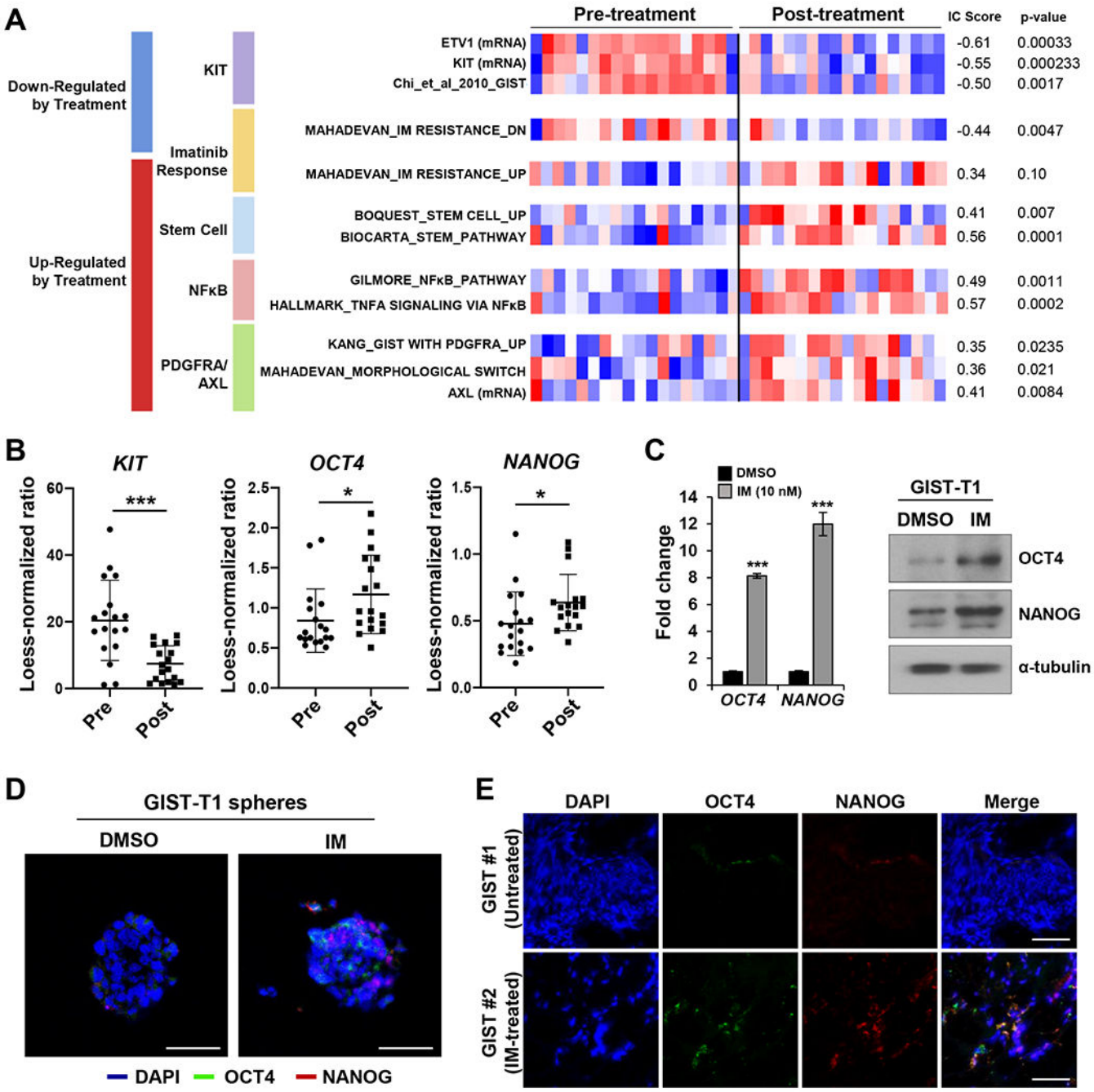

FIG. 1. IM increases expression of stem markers in human GIST

A. Gene Set Enrichment Analysis (GSEA) analysis(53) performed on 18 paired pre-IM vs. post-IM samples from RTOG 0132.(78) Selected gene sets that show differential enrichment before and after IM treatment. The heatmap displays the standardized enrichment scores of a variety of gene sets representing KIT activation, imatinib resistance, stemness, NF-κB, and PDGFRA/AXL. On the left side of the heatmap, the numbers display the association metric (IC score(40), and the p-values obtained by performing an empirical permutation test. Red: above mean; blue: below mean). **B.** Transcript expression differences among

stem-associated transcription factors and *KIT* from RTOG0132 microarray data. *** and * represent statistical significance P<0.001 and P<0.05, respectively. **C.** Relative expression levels of stem markers by RT-PCR analysis and protein levels by Western blots in GIST-T1 tumorspheres treated with IM (10 nM) for 3 days. RT-PCR data performed in triplicates were shown as mean ± standard deviation (SD). Alpha-tubulin was used as a Western blot loading control. **D.** Protein levels of stem markers by immunofluorescent (IF) staining in GIST-T1 spheres treated with 100 nM IM for 7 days. **E.** Representative IF staining for co-localization of stem markers comparing untreated GIST #1 and IM-treated *KIT* exon 11 mutated GIST #2.

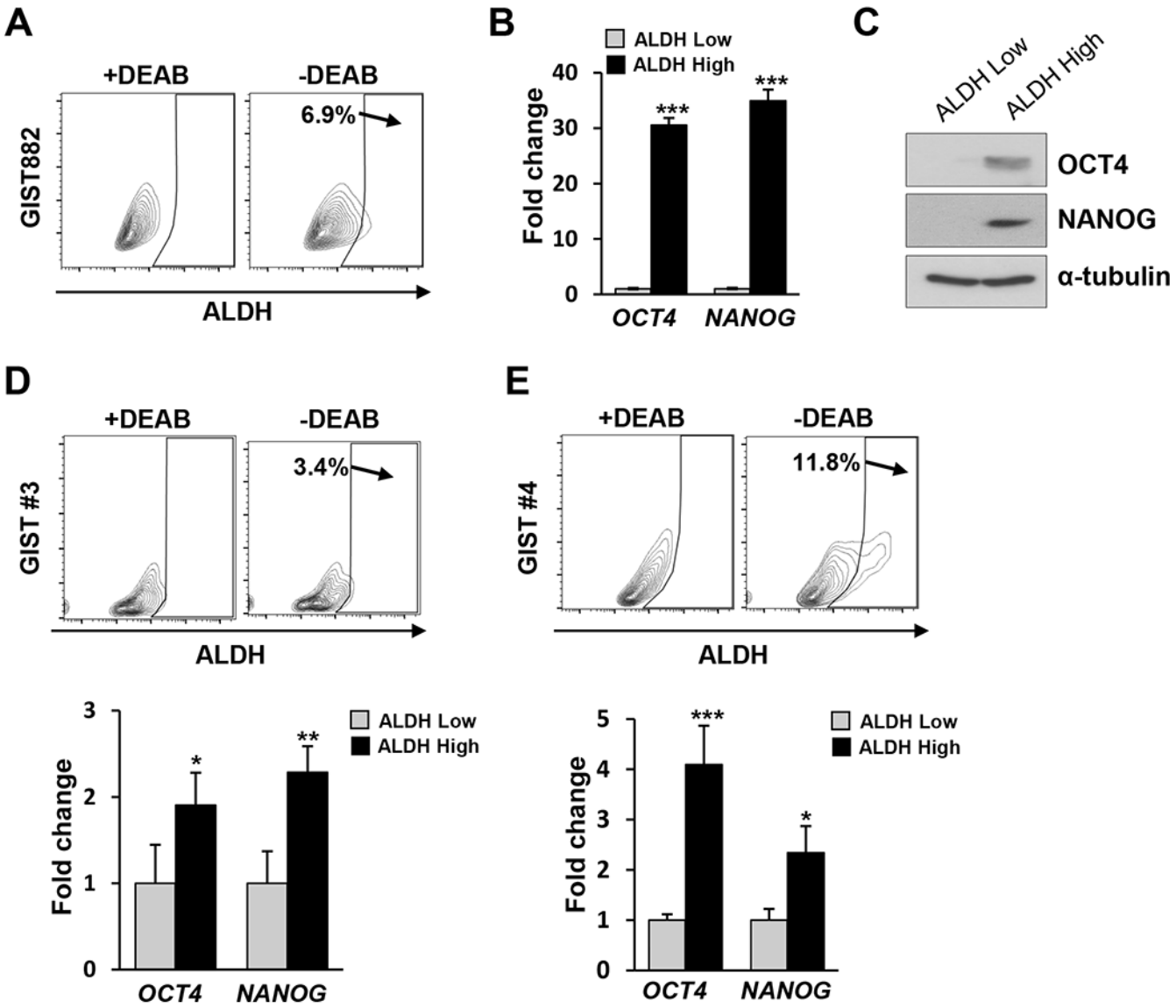

FIG. 2. Treatment naïve GIST cells have properties of "stemness"

A. Specific ALDH fluorescent intensity was detected by FCM in GIST882 with or without ALDH inhibitor DEAB. **B.** Bar graphs displayed relative expression level of stem markers by RT-PCR analysis in sorted ALDH^{high} and ALDH^{low} (set as 1-fold baseline) cells from GIST882. Data shown as mean ± SD was performed in triplicate. **C.** Immunoblots showed protein levels of stem markers in GIST882 from sorted ALDH^{high} and ALDH^{low} cells. Alpha-tubulin was used as a loading control. **D.-E.** Two *KIT*-mutant GIST analyzed by FCM for ALDH fluorescent intensity in the presence or absence of DEAB. Bar graphs showed RT-PCR data of sorted ALDH^{high} and ALDH^{low} (set as 1-fold baseline) from both GIST for OCT4 and NANOG relative expression. Data performed in triplicate was shown as mean ± SD. Statistical significance is indicated by *** P<0.001, ** P<0.01, and * P<0.05.

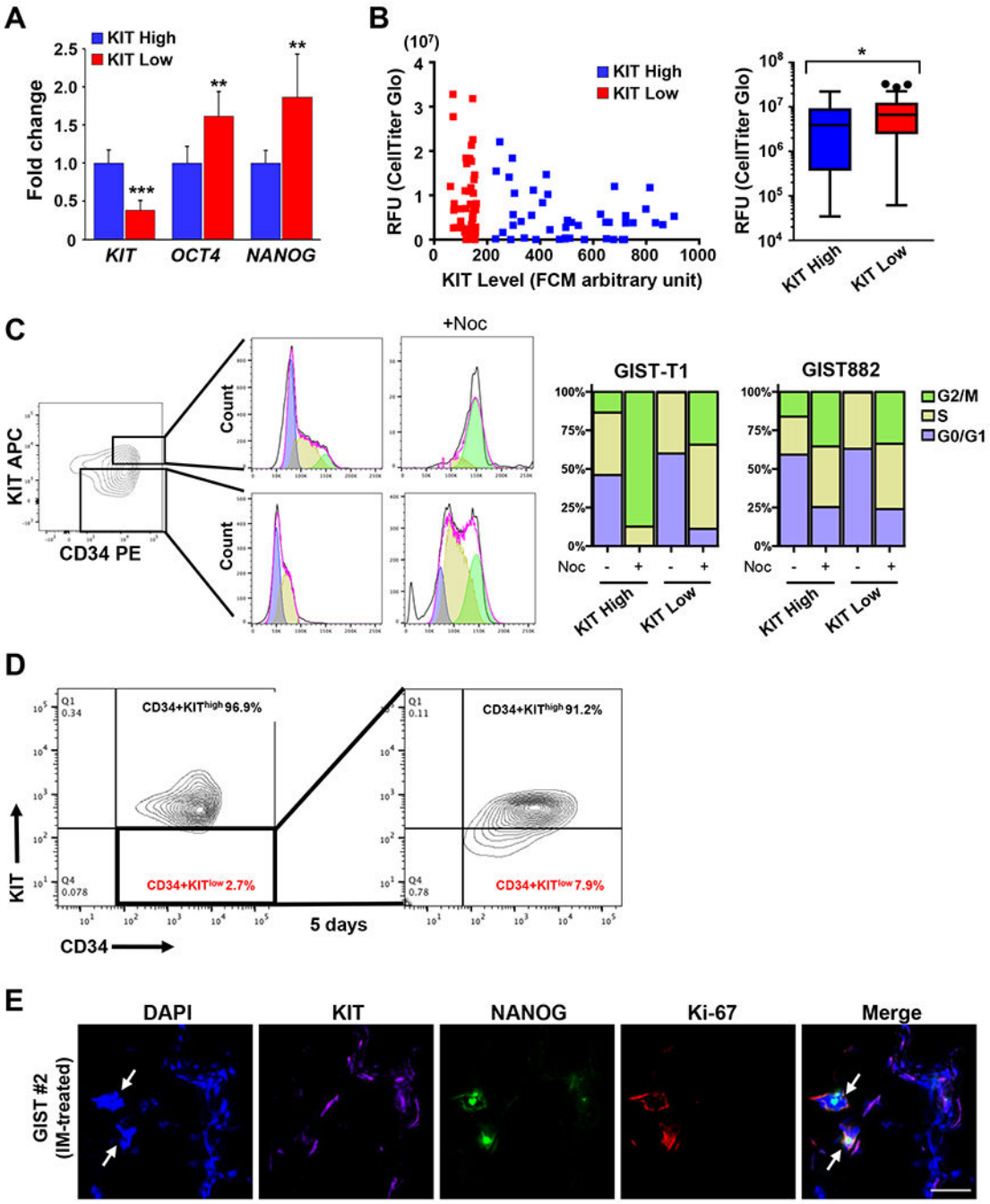

FIG. 3. KIT^{low} GIST cells are stem cell-like

A. Relative expression level of stem markers (*OCT4* and *NANOG*) and *KIT* by RT-PCR analysis in sorted GIST882 KIT^{high} and KIT^{low} cells. Data performed in triplicate are shown as mean ± SD. *** P<0.001 and ** P<0.01. **B.** Cell viability displayed in relative fluorescence units (RFU) was determined by CellTiter-Glo assay in sorted GIST882 KIT^{high} and KIT^{low} cells based on their fluorescence intensity. Box plots show the average RFU for sorted populations. *represents statistical significance P=0.042 by Mann-Whitney test. Three outliers were indicated by black dots. **C.** FCM contour plot show sorted KIT^{high} and KIT^{low}

cells inside the top and bottom boxed areas, respectively, that were collected and treated with DMSO or the microtubule inhibitor nocodazole (+Noc) for 24 hours. FCM histograms and bar graph show cell distribution within the cell cycle phases namely, G0/G1, S-phase and G2/M, from DMSO- or Noc-treated KIT^{high} and KIT^{low} cells. **D.** FCM contour plots showed the percentages of KIT^{high} and KIT^{low} cells that were derived from GIST882 KIT^{low} cells (inside the boxed area) from the first sorting after culturing in regular growth media for 5 days. **E.** Representative IF staining for co-localization of KIT, NANOG, and Ki67 from IM-treated *KIT* exon 11 mutated GIST#2. Arrows indicate KIT^{low} cells expressing both NANOG and Ki-67.

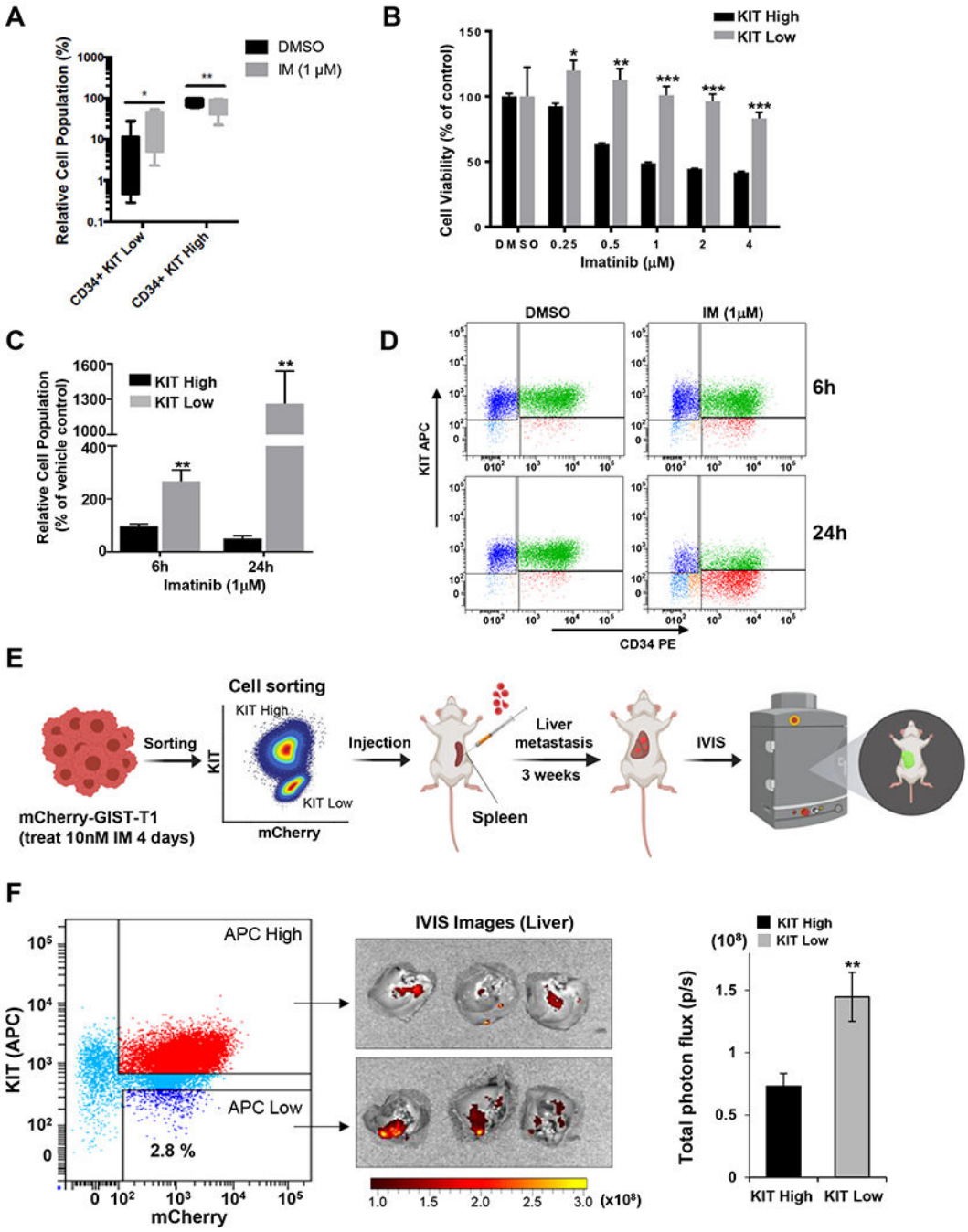

FIG. 4. TKI treatment enriches for KIT^{low} GIST cells

A. GIST882 cells were treated with 1 μM IM for 48 hours. FCM analysis performed on treated and untreated cells. Box-and-whisker plots depict median values ± standard deviation. **B.** GIST882 cells underwent FACS to separate KIT$^{high/low}$ populations. Cell viability of sorted KIT^{high} and KIT^{low} cells treated with indicated doses of IM for 72 hours. DMSO-treated cells were set as 100% viability. Statistical significance is indicated by *** P<0.001, ** P<0.01, and * P<0.05. **C.** Relative cell population from sub-groups of KIT^{high} and KIT^{low} cells after treated GIST882 with 1μM IM for 6 or 24 hours and determined by

FCM. Counts from cells treated with DMSO in each group at each time point were set as the baseline (100%). ** P<0.01. **D.** Representative FCM dot plots showed the sub-groups of KIT^{high} and KIT^{low} cells from GIST882 cells 6- or 24-hr post-treatment with 1 μM IM. **E.** Flowchart diagram for *in vivo* testing of sorted KIT^{high} and KIT^{low} from mCherry-GIST cells pre-treated with 10nM IM for 4 days in a liver metastasis model. **F.** FCM dot plot displayed cell sorting for KIT^{high} and KIT^{low} from mCherry-T1 cells. IVIS images of the whole liver were obtained from all animals. Bar graph showed the liver metastasis quantified by the total photon flux (p/s). ** P<0.01.

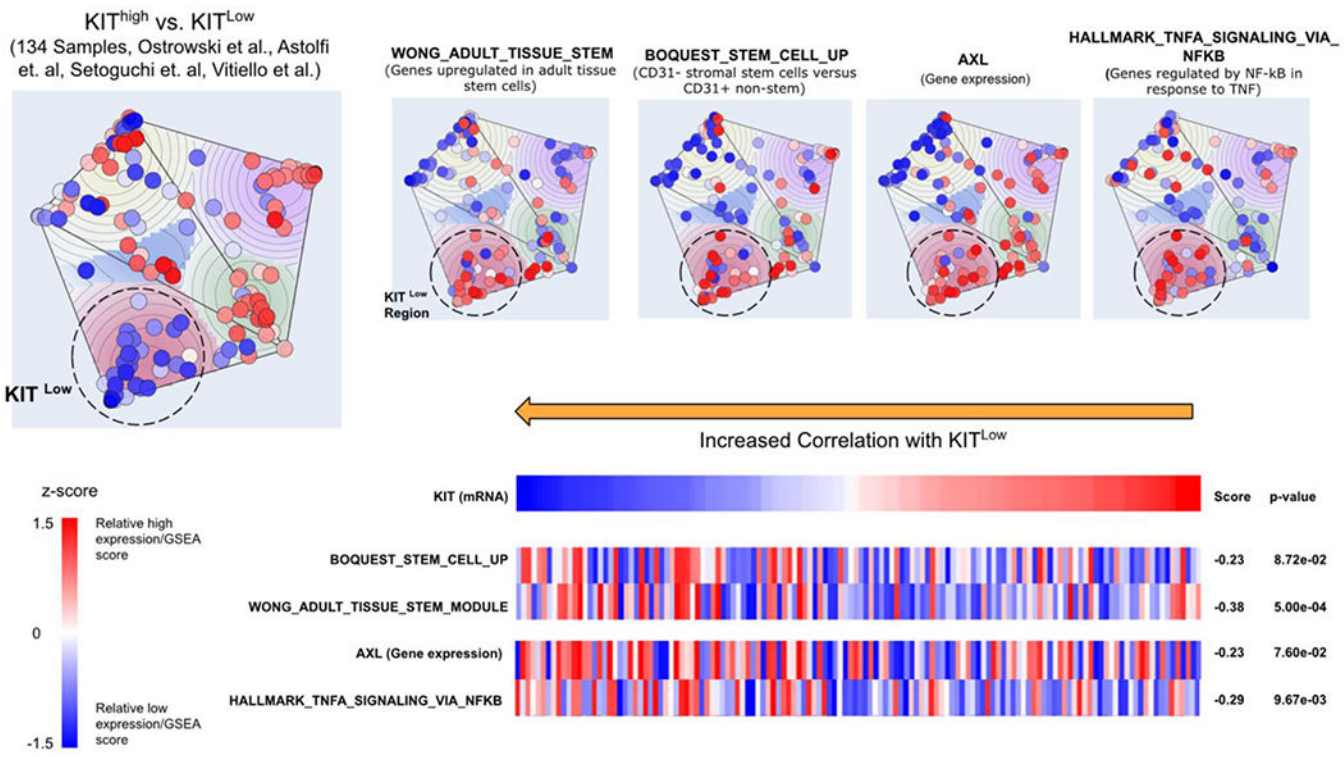

FIG. 5. KIT^{low} primary tumors have distinct pathway activation

Onco-GPS map constructed using gene expression of 134 GIST samples from 4 datasets. Relative gene expression and gene set enrichment scores are shown on the map by coloring projected samples on a scale of blue for low enrichment and red for high enrichment of each indicated gene or pathway. Indicated genes and pathways are also shown in the left panel showing the matching score (Information Coefficient) against *KIT* mRNA expression.

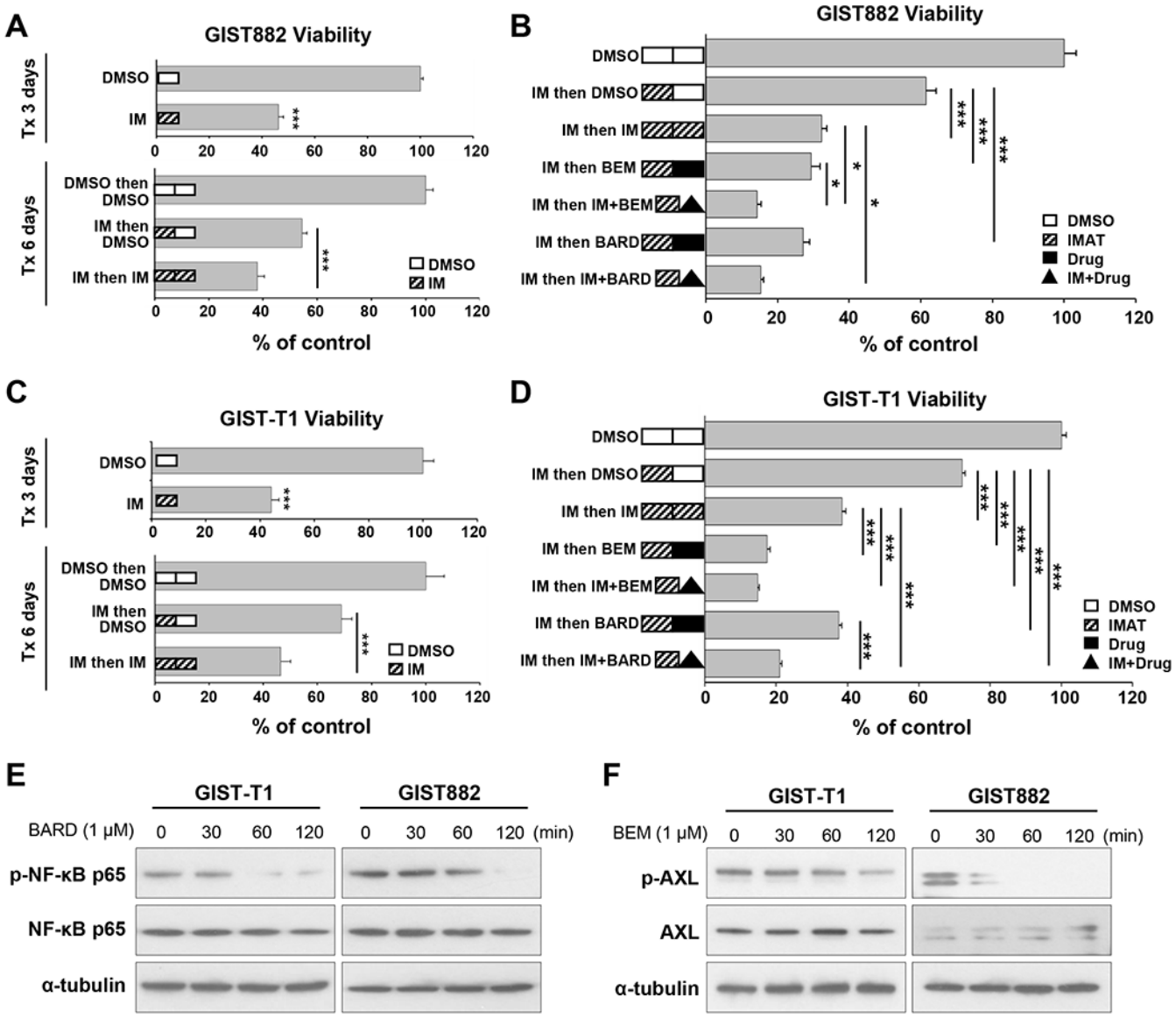

FIG. 6. Combination drug treatment is cytotoxic in IM-resistant GIST

A. Cell viability for GIST882 cells in sequential treatment experiments with 300 nM IM (dose selected based on IC_{75}). Some cells were treated for a total of 6 days. After 3-day IM treatment (i.e. Days 1-3), remaining cells in wells were refreshed with new media containing DMSO or IM then cultured for an additional 3 days (i.e. Days 4-6). For the 3-day group, cells treated with DMSO were set as controls of 100% viability; whereas controls for the 6-day group were cells in DMSO from Days 1-3 then in DMSO from Days 4-6. **B.** Cell viability for GIST882 cells treated with 185 nM IM (dose selected based on IC_{50}) followed by various compounds in sequential treatment experiments. After 3-day IM treatment (i.e. Days 1-3), remaining cells were refed with fresh media containing DMSO, 185nM IM, 1μM BARD, 1 μM BEM, or combination of IM and indicated drugs were then cultured for an additional 3 days (i.e. Days 4-6). **C.** Cell viability for GIST-T1 cells in sequential treatment experiments with 20 nM IM (dose selected based on IC_{75}). Some T1 cells underwent 6-day

treatment as described above in (A) for GIST882 cells. **D**. Cell viability for GIST-T1 cells with 20 nM IM treatment for 3 days then followed with various compounds and 20 nM IM in sequential treatment as described above in (B) for GIST882 cells. DMSO-treated cells (for total 6 days) were set as 100% viability controls. Statistical significance is indicated by *** $P<0.001$ and * $P<0.05$. **E**. GIST cells were treated with 1μM BARD for indicated time and lysed for Western blotting to detect total NF-kB p65 protein and phospho-NF-kB p65 (Ser536). **F**. Immunoblots from GIST cells treated with 1μM BEM for indicated time and probed for total AXL and phosphor-AXL. Alpha-tubulin was used a loading control.

Table 1:

Characteristics of primary human GISTs

Tumor Name	Primary Site	Mutation
GIST #1	Gastric	*KIT* exon 11 V560E
GIST #2	Gastric	*KIT* exon 11 V560E
GIST #3	Gastric	*KIT* exon11 R586 N587_ins^{PTQLPYDHKWEFPR}
GIST #4	Gastric	*KIT* exon11 V560D